Inertial range Eulerian and Lagrangian statistics from numerical simulations of isotropic turbulence

R. BENZI[1], L. BIFERALE[1]†, R. FISHER[2], D. Q. LAMB[3] AND F. TOSCHI[4]

[1]Department of Physics and INFN, University of Rome Tor Vergata,
Via della Ricerca Scientifica 1, 00133 Rome, Italy

[2] Department of Physics, University of Massachusetts at Dartmouth,
285 Old Westport Road, Dartmouth, MA 02740, USA

[3] Center for Astrophysical Thermonuclear Flashes, The University of Chicago,
Chicago, IL 60637, USA and Department of Astronomy and Astrophysics,
The University of Chicago, Chicago, IL 60637, USA

[4] Department of Physics and Department of Mathematics and Computer Science,
Eindhoven University of Technology, 5600 MB Eindhoven, The Netherlands
and Istituto per le Applicazioni del Calcolo CNR, Viale del Policlinico 137,
00161 Rome, Italy

We present a study of Eulerian and Lagrangian statistics from a high-resolution numerical simulation of isotropic and homogeneous turbulence using the FLASH code, with an estimated Taylor microscale Reynolds number of around 600. Statistics are evaluated over a data set with 1856^3 spatial grid points and with $256^3 = 16.8$ million particles, followed for about one large-scale eddy turnover time. We present data for the Eulerian and Lagrangian structure functions up to the tenth order. We analyze the local scaling properties in the inertial range. The Eulerian velocity field results show good agreement with previous data and confirm the puzzling differences previously found between the scaling of the transverse and the longitudinal structure functions. On the other hand, accurate measurements of sixth-and-higher-order Lagrangian structure functions allow us to highlight some discrepancies from earlier experimental and numerical results. We interpret this result in terms of a possible contamination from the viscous scale, which may have affected estimates of the scaling properties in previous studies. We show that a simple bridge relation based on a multifractal theory is able to connect scaling properties of both Eulerian and Lagrangian observables, provided that the small differences between intermittency of transverse and longitudinal Eulerian structure functions are properly considered.

1. Introduction

In the last few years, many interesting and remarkable results have been obtained by investigating the statistical properties of Lagrangian particles advected by a turbulent flow; see for instance the recent review by Toschi & Bodenschatz (2009). For the purposes of this paper, we will consider Lagrangian tracers to be idealized

† Email address for correspondence: biferale@roma2.infn.it

point-like particles, whose instantaneous velocity coincides with the local Eulerian velocity field, $u(x, t)$: $\dot{X}(t) = u(X(t), t)$. The study of fully developed turbulence in a Lagrangian framework clearly has many immediate applications, where the transport and/or aggregation of material particles embedded in the flow field is important. Furthermore, the study of fully developed turbulence in the Lagrangian framework has opened important new directions in purely scientific investigations. In particular, the small-scale intermittency of turbulent flows and the nature of the dissipation range can be probed more effectively in the Lagrangian framework than in the Eulerian framework, as has been shown recently in both experiments and in numerical simulations (see for instance Yeung & Pope 1989; Ott & Mann 2000; La Porta *et al.* 2001; Mordant *et al.* 2001; Biferale *et al.* 2005; Luethi, Tsinober & Kinzelbach 2005; Berg *et al.* 2006; Bourgoin *et al.* 2006; Mordant, Lévêque & Pinton 2006; Yeung, Pope & Sawford 2006; Homann *et al.* 2007; Berg *et al.* 2009; Homann *et al.* 2009). (See also Biferale *et al.* 2008 and Arneodo *et al.* 2008 for comparison between experimental and numerical Lagrangian data.) Lagrangian and Eulerian measurements are intimately connected via their corresponding statistical description of the same underlying flow; another goal of this paper is to quantitatively determine the degree of correlation between the two ensembles.

In this paper, we present new results concerning the statistical properties of inertial-range Lagrangian and Eulerian velocity fields in a homogeneous and isotropic fully developed turbulent flow. The flow itself is the outcome of a high-resolution weakly compressible numerical simulation, which is both described and subsequently validated in §2 . Our motivation in this study is twofold. First, thanks to both the relatively high spatial resolution of the Eulerian mesh and the large numbers of tracer particles – some 16 million particles, which makes this 'the largest Lagrangian data set currently available for fully developed homogeneous and isotropic turbulence' – we are able to extract the statistics of the Lagrangian velocity field with high accuracy and relatively small error bars. We assess, for the first time at this Reynolds number, statistical fluctuations 'scale-by-scale' in the Lagrangian inertial range as intense as those given by moments up to order 10. Secondly, as a side result of this validation procedure, we also show that the weakly compressible nature of the code does not affect the Eulerian and Lagrangian velocity field in the inertial range. We demonstrate this result by direct quantitative comparison with (i) numerical results obtained with pseudo-spectral code, (ii) experimental results of incompressible flows and (iii) an exact relation valid for Navier–Stokes equations of incompressible flows.

Our second motivation deals with the statistical link between Lagrangian and Eulerian measurements. We show that a simple model, based on the multifractal theory, is able to translate between the two ensembles with good quantitative agreement (see Borgas 1993; Boffetta, De Lillo & Musacchio 2002 for the first theoretical developments and Chevillard *et al.* 2003; Biferale *et al.* 2004; Arneodo *et al.* 2008 for further numerical and experimental verification).

Our main tool in analyzing our Lagrangian data is the numerical computation of velocity increments over a time lag τ – the so-called Lagrangian structure functions (LSFs):

$$\mathscr{S}_i^{(p)}(\tau) = \langle [v_i(t + \tau) - v_i(t)]^p \rangle = \langle (\delta_\tau v_i)^p \rangle, \qquad (1.1)$$

where $i = x, y, z$ are the three velocity components along a particle trajectory, $v_i(t) = u_i(x(t), t)$ and the average is defined over the ensemble of particle trajectories. In a stationary and homogeneous flow, all moments of the velocity increments depend solely on the time lag τ. When the flow is also isotropic, all components

must be symmetric; we will therefore drop the dependency on the spatial index here. In the inertial range, for time lags smaller than the integral time and larger than the Kolmogorov time, $\tau_\eta \ll \tau \ll T_L$, nonlinear energy transfer governs the dynamics. From a dimensional viewpoint, only the scale τ and the energy transfer ϵ should enter into the structure functions (SFs). The only admissible choice in isotropic statistics is therefore $\mathscr{S}^{(p)}(\tau) \sim (\epsilon\tau)^{p/2}$. However, this choice does not take into account the fluctuating nature of dissipation due to intermittency. Many empirical studies (see Toschi & Bodenschatz 2009 for a recent review) have indeed shown that the tail of the probability density functions (p.d.f.) of $\delta_\tau v$ becomes increasingly non-Gaussian at decreasing τ/T_L, leading to intermittency and anomalous scaling exponents, meaning a breakdown of the dimensional law, i.e.

$$\mathscr{S}^{(p)}(\tau) \sim \tau^{\xi^{(p)}}, \tag{1.2}$$

with $\xi^{(p)} \neq p/2$.

As we will review and test in detail later in this paper, the Lagrangian measurements can be linked to the Eulerian structure functions (ESFs). In isotropic statistics we may have two different Eulerian increments, longitudinal and transverse (see Frisch 1995 for a textbook introduction to scaling in homogeneous and isotropic turbulence):

$$\left.\begin{aligned} S_L^{(p)}(r) &\equiv \langle [\boldsymbol{u}(\boldsymbol{x}+\boldsymbol{r}) - \boldsymbol{u}(\boldsymbol{x})] \cdot \hat{\boldsymbol{r}}]^p \rangle, \quad \hat{\boldsymbol{r}} = \boldsymbol{r}/|\boldsymbol{r}|, \\ S_T^{(p)}(r) &\equiv \langle |\boldsymbol{u}(\boldsymbol{x}+\boldsymbol{r}_T) - \boldsymbol{u}(\boldsymbol{x})|^p \rangle, \quad \boldsymbol{r}_T \cdot \boldsymbol{u} = 0. \end{aligned}\right\} \tag{1.3}$$

It is well established (Frisch 1995; Arneodo *et al.* 1996) that Eulerian statistics also exhibit anomalous scaling, for $\eta \ll r \ll L$:

$$\left.\begin{aligned} S_L^{(p)}(r) &\sim r^{\zeta_L^{(p)}}, \\ S_T^{(p)}(r) &\sim r^{\zeta_T^{(p)}}. \end{aligned}\right\} \tag{1.4}$$

From a theoretical point of view, in isotropic turbulence one would expect that longitudinal and transverse fluctuations have the same scaling, $\zeta_L^{(p)} = \zeta_T^{(p)}$ (see Biferale & Procaccia 2005 for a review on anisotropic turbulence). This is not what was observed in some experimental and numerical analyses (Boratav & Pelz 1997; Chen, Sreenivasan & Nelkin 1997; Dhruva, Tsuji & Sreenivasan 1997; van de Water & Herweijer 1999; Zhou & Antonia 2000; Shen & Warhaft 2002). This discrepancy can be due to either finite Reynolds numbers (He *et al.* 1998; Hill 2001) or some remnant small-scale anisotropy (Biferale & Procaccia 2005). Still, even large Reynolds numbers direct numerical simulation (DNS) with isotropic forcing show some persistent differences between $\zeta_L^{(p)}$ and $\zeta_T^{(p)}$, as shown in Gotoh, Fukayama & Nakano (2002) and Ishihara, Gotoh & Kaneda (2009). The same discrepancy between the longitudinal and transverse velocity SFs is quantitatively confirmed in the analysis reported here. Whether this effect will persist at higher Reynolds number remains an important open question for further experimental and numerical investigations. In addition, the analysis of our data is also directly relevant to a broad class of numerical simulation methods common in astrophysics and in atmospheric physics, which model the Euler equations of hydrodynamics but inevitably implicitly introduce numerical dissipation near the grid scale. These simulation methods are sometimes referred to as implicit LES simulations (ILES) to properly distinguish them from DNS simulations of the Navier–Stokes equations. This fact leads to interesting issues in our discussion. In particular, because the FLASH code does not dissipate energy in the same manner as a DNS simulation of the Navier–Stokes equations (see §2 for

details) implies that the observed inertial range discrepancy between longitudinal and transverse scaling, which is common to simulations using both approaches, is very unlikely to be caused by viscous effects.

With regard to the issue of Lagrangian intermittency, a 'bridge relation' between Lagrangian and Eulerian inertial range exponents has been recently proposed on the basis of a common multifractal description (Borgas 1993; Boffetta *et al.* 2002). This bridge relation has proved to be very efficient in predicting the p.d.f. of Lagrangian accelerations (Biferale *et al.* 2004). Previous work has verified the bridge relation up to the fourth-order moment of the Lagrangian velocity SF (Arneodo *et al.* 2008). On the other hand, previous measurements of higher-order LSF (Mordant *et al.* 2006; Xu *et al.* 2006) do not agree with the inertial range bridge relation. Also, a similar relation bridge written for MHD turbulence does not seem to apply Homann *et al.* (2009). It is therefore important to test it up to high-order moments with high statistical accuracy. Here, we show that the multifractal bridge relation is indeed valid up to moment of order 'ten' for homogeneous and isotropic turbulence, the highest moment measurable with an acceptable signal-to-noise ratio in our data. We interpret the discrepancy with previous results as due to a possible contamination from the viscous scale affecting the estimate of the scaling properties in Mordant *et al.* (2006); Xu *et al.* (2006), see table 2 and related discussion.

Finally, we also discuss the theoretical implications of multifractal phenomenology for viscous time fluctuations in the Lagrangian domain and deal with finite Reynolds effects, the importance of vortex trapping and the dependency on the multifractal spectrum for smooth inertial range fluctuations.

The paper is organized as follows. In §2 we discuss the numerical simulation, the resulting data set and its corresponding validation. In §3 we discuss the computation of the ESFs. In §4 we report the analysis of LSF and discuss the physical results obtained by our analysis. In §5 we provide a theoretical interpretation of our findings by employing the multifractal framework. Conclusions follow in §6.

2. Data set and numerical simulations

As briefly highlighted in the introduction, our main purpose is to investigate intermittency of the Lagrangian and Eulerian velocity fields in the inertial range for homogeneous and isotropic turbulent flow (see figure 1 for a colour rendering). The numerical simulations have been performed using the FLASH code developed by the Flash Center at the University of Chicago (Fisher *et al.* 2007). The Euler inviscid equations of hydrodynamics solved by the code are:

$$\left. \begin{aligned} &\partial_t \rho + \nabla \cdot (\boldsymbol{u}\rho) = 0, \\ &\partial_t (\rho \boldsymbol{u}) + \nabla \cdot (\boldsymbol{u}\boldsymbol{u}\rho) = -\nabla P + \boldsymbol{F}, \\ &\partial_t (\rho E) + \nabla \cdot [\boldsymbol{u}(\rho E + P)] = 0, \\ &P = (\gamma - 1)\rho U, \\ &E = \rho(U + \tfrac{1}{2}u^2), \end{aligned} \right\} \tag{2.1}$$

where ρ is the mass density, $\boldsymbol{u}$ is the velocity, P is the pressure, E is the total energy density, U is the specific internal energy and γ is the ratio of the specific heats in the system. Finally, the fourth equation in (2.1) is the equation of state closing the system. The effect of the large-scale forcing $\boldsymbol{F}$ gives rise to a turbulent flow whose energy is transferred from scale L_0 towards small scales. The energy input $\int \mathrm{d}^3 x \, \boldsymbol{u} \cdot \boldsymbol{F}$ produces an increase of the internal energy U, which grows in time. One can easily show that

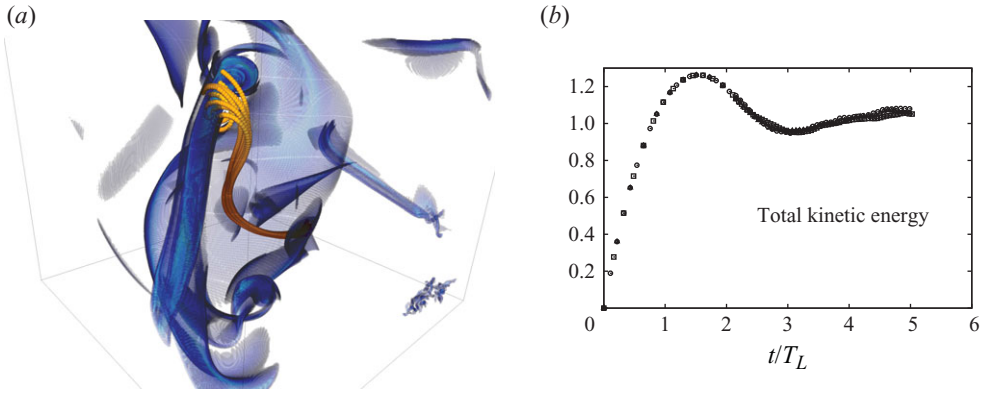(*a*)   (*b*)

FIGURE 1. (*a*) Example of Eulerian and Lagrangian rendering. Both the intensity of the Eulerian enstrophy field at a given time (blue isosurface) and the Lagrangian evolution of a bunch of particles with trajectories ending at the time of the Eulerian snapshot are shown. Notice that the Lagrangian particles have an initially smooth evolution because we also show the initial transient time when the underlying Eulerian field was chosen smooth and with low energy. The bunch of particles was chosen such as to encounter a vortex filaments during their evolution. Figure by courtesy of B. Gallagher. (*b*) Evolution of the total kinetic energy for each component, $\langle (u_i)^2 \rangle /2$, with $i = x, y, z$ during the whole run, including the initial transient. Notice the good isotropy of the run, which makes the three symbols referring to the three different components almost undistinguishable. In the paper, all Eulerian and Lagrangian statistical data are measured only after stationarity is reached, $t/T_L > 3$.

the quantity $\int \mathrm{d}x^3 P \, \partial_i v_i$ represents the energy transfer from kinetic to internal energy of the flow. The sound speed increases in time as well, while the average Mach number is of order 0.3. The numerical simulation is isotropic and homogeneous forcing with a resolution 1856^3. The integration in time has been done for three eddy turnover times after a transient evolution (see figure 1 for the evolution of the total kinetic energy in the flow).

The stirring is obtained by a divergence-free, time-correlated momentum source term on all wavenumbers with $|k| \leqslant 4$, using an algorithm originally proposed by Eswaran & Pope (1988). For each mode at each time step, six complex phases (real and imaginary in each of the three spatial dimensions) are evolved by an Ornstein-Uhlenbeck coloured-noise stochastic differential equation. By evolving the phases of the stirring modes in Fourier space, imposing a divergence-free condition is relatively straightforward. At each time step the solenoidal component of the velocities is projected out, leaving only the non-compressional modes to add to the velocities. The velocities are then converted to physical space by a direct Fourier transform. FLASH includes a directionally split piecewise parabolic method (PPM) solver descended from the PROMETHEUS code as proposed in Colella & Woodward (1984) and Arnett, Fryxell & Mueller (1989). It is a higher-order version of the Godunov method, representing flow variables with piecewise parabolic functions within cells. It also uses a set of monotonicity constraints rather than artificial viscosity to control oscillations near discontinuities, including both strongly sheared interfaces and contact surfaces as well as shocks. The high resolution and accuracy of PPM are obtained by the explicit nonlinearity of the scheme and through the use of dissipation algorithms, such as monotonicity enforcement and interpolant flattening, which are tailored to activate only in the immediate vicinity of discontinuities. More details on the numerical code can also be found in Benzi *et al.* (2008) and §2.1 below. About

16 million separate Lagrangian tracers have been evolved together with the Eulerian fields. Particle velocities are obtained by quadratic interpolation of the Eulerian hydrodynamic velocity field at the particle position. A standard second-order Runge–Kutta algorithm was used for the time integration scheme. The code develops density gradients due to compressibility. Despite compressible effects, which lead to non-trivial scaling of density and entropy fluctuations (Porter, Pouquet &. Woodward 2002; Benzi *et al.* 2008), the net feedback on the velocity scaling is very weak, if any.

2.1. *Validation of the numerics*

The FLASH code is the product of nearly a decade of intensive software development, including careful attention to code verification and validation (Rosner *et al.* 2000). Different validation studies on problems, as diverse as Richtmyer–Meshkov and Rayleigh–Taylor instabilities (Calder *et al.* 2002), shock–cylinder interaction (Weirs *et al.* 2005) and laser-driven high energy density laboratory experiments (Kane *et al.* 2001), have been performed in the past. The code has also been applied to study buoyancy-driven turbulent combustion (Zhang *et al.* 2007), wind-driven instabilities in neutron star atmospheres (Alexakis *et al.* 2004), type Ia supernovae (Plewa, Calder & Lamb 2004) and many other astrophysical flows.

   In the following, we show that to the best of our testing ability, in the simple homogeneous isotropic case investigated here, without coupling to chemical or combustion effects, the Lagrangian and Eulerian velocity fluctuations in the inertial range are indistinguishable from those measured in incompressible fluid turbulence. The only appreciable differences can be captured for viscous scales, where one is forced to define an 'effective viscosity' and an effective 'dissipative scale' to compare with Navier–Stokes results. Although the integration is formally inviscid, there is a net energy transfer from the turbulent kinetic energy $1/2\rho u^2$ to the internal energy. Thus, we may think that an effective viscosity ν_{eff} is acting on the system. In order to estimate the effective viscosity, we proceed as if the Kolmogorov 4/5 equation (see Frisch 1995) – valid for incompressible turbulence – applies to our case, with effective parameters:

$$S_L^{(3)}(r) = -\frac{4}{5}\epsilon_{eff}r + 6\nu_{eff}\frac{\mathrm{d}}{\mathrm{d}r}S_L^{(2)}(r). \tag{2.2}$$

A fit of our data with this formula gives, $\epsilon_{eff} = 0.054$, $\nu_{eff} = 8.3 \cdot 10^{-6}$, which corresponds to a Kolmogorov scale, $\eta = (\nu_{eff}^3/\epsilon_{eff})^{1/4}$, equivalent to roughly half a grid cell in units where the total box size is $L = 1$, and to a microscale Reynolds number $R_\lambda \sim 600$. The dynamical effects of the effective viscosity present here is, however, different from what one usually observes in the Navier–Stokes equations, i.e. the dissipation range does not behave similarly to the Navier–Stokes solutions. Thus, while on the energy flux (i.e. the third-order SFs) we still observe an effective dissipation. The dissipation range is changed according to the specific mechanism employed in the simulation. One may thus have problems in assessing correlation between particle trajectories and viscous-scale fields as vorticity and strain, in the spirit of the refined Kolmogorov hypothesis translated to the Lagrangian domain (Benzi *et al.* 2009). Because our main interest here is to describe inertial range physics, the uncertainty in defining the exact value of the viscous cut-off is unimportant.

   In inertial range quantities, the physics get closer to Navier–Stokes equations. We discuss hereafter these inertial range properties using analytic, numerical and experimental validation. For isotropic and incompressible flows described by the Navier–Stokes equations, there exists an exact relation which connects second-order
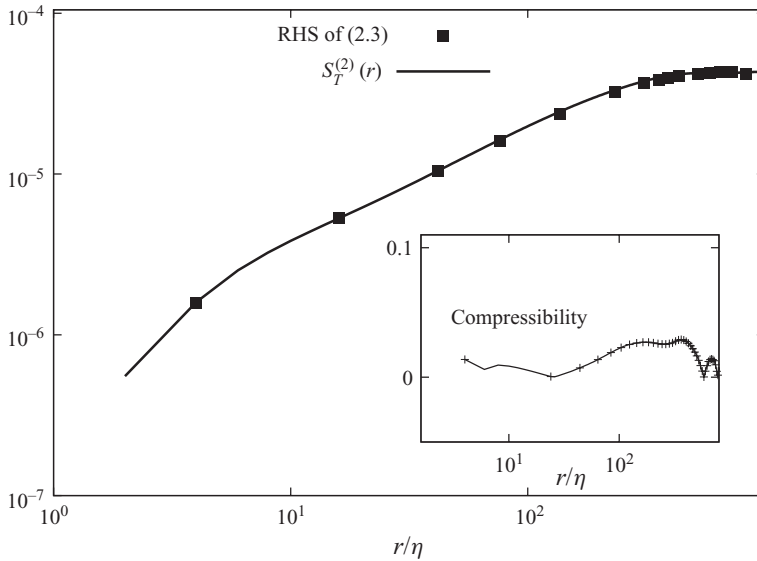
FIGURE 2. Test of the isotropic and incompressible constraint, we show the left-hand side (LHS) and the right-hand side (RHS) of (2.3). Inset, a percentage estimate of the breaking of the relation: (RHS − LHS)/LHS. Notice that percentagewise the relation is well verified, within 5 % of accuracy.

longitudinal and transverse SFs (Frisch 1995):

$$S_T^{(2)}(r) = S_L^{(2)}(r) + \frac{r}{2}\frac{\mathrm{d}}{\mathrm{d}r}S_L^{(2)}(r); \qquad (2.3)$$

this equation is useful because any deviations from it give a quantitative hint on the cumulative importance of anisotropy and compressibility, scale-by-scale. We show in figure 2 the comparison between $S_T^{(2)}(r)$ and its reconstruction via the right-hand side of (2.3). As one can see, the agreement is very good. In the inset of the same figure we show that combined effects due to anisotropy and compressibility are less than a few percent for second-order statistics (see also figure 4 for higher-order statistics). Moreover, it is well known that third-order longitudinal SFs in isotropic, homogeneous and incompressible turbulence obeys the 4/5 law: $S_L^{(3)}(r) \sim r$, which is the only exact result involving non-trivial dynamical properties known for fully developed turbulence. In figure 3 we show the third-order longitudinal ESF as measured in our numerics. As one can see there is a clean scaling range over more than one decade extending from $r/\eta \in [10{:}100]$, with a slope close to the scaling prediction. Both these comparisons with exact inertial range results for incompressible Navier–Stokes equations show us that the velocity field in the FLASH code does not present important compressibility effects (a simple worst-case estimate based on the Mach number would indeed suggest effects within 9 %).

Two additional papers recently published further extend the validation study presented here. In the first, we have quantitatively compared the inertial range local slopes of ESFs as measured with our code with those obtained from a pseudo-spectral incompressible code (see figure 1 of Benzi *et al.* 2008). An additional, even more stringent, test was also recently completed for the Lagrangian statistics. A joint collaboration of 28 scientists put together all currently existent Lagrangian data concerning second- and fourth-order SFs, the results of three different experiments
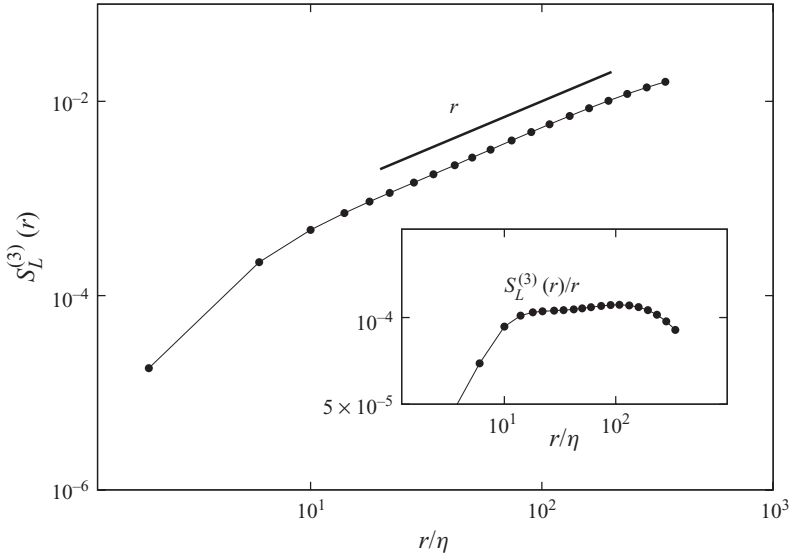
FIGURE 3. Third-order longitudinal SF, $S_L^{(3)}(r)$ with the power law exact relation coming from the 4/5 law (Frisch 1995). Inset, compensated plot, $S_L^{(3)}(r)/r$.

and five different numerical simulations (four pseudo-spectral and the one obtained by using our FLASH code). As shown in figure 1 of Arneodo *et al.* (2008), all data are consistent with one another, and, more importantly, the FLASH data set is the one with the smallest statistical and systematic errors, thanks to the high number of particle trajectories integrated numerically.

3. Intermittency and anomalous scaling in the Eulerian inertial range

We start our analysis by measuring the scaling behaviour of the ESFs. In figure 4 we show a typical log–log plot of longitudinal ESF for $p = 2, 6, 10$. A qualitative scaling behaviour is clearly detectable. In figure 4(*b*), we show the estimate of the statistical fluctuations by showing the effects of halving the sample size, i.e. plotting the ratio between two structure functions averaged over the whole statistics or over one half of it. As one can see, statistical fluctuations become, at the maximum, of order 10–20 % at small scales (where intermittency is more severe) and only for high-order moments $p = 6$ and larger. Inside the inertial range, $r > 10\eta$, they are of order 5 % or even less. Similarly, in figure 4(*c*) we give a quantitative estimate of residual anisotropy, by plotting the ratio between longitudinal measurements over two different orthogonal directions. Here, as expected, deviations are larger close to the integral scale, reaching a maximum of 10 % for high-order moments. As a result, the combined effect of statistical and anisotropic fluctuations for the Eulerian scaling is small, and it results in an estimate of the error bars that are within the size of the symbols for the log–log plot showed in figure 4(*a*).

One of the advantages of high spatial resolution is the possibility to go beyond log–log plots, analyzing scaling properties 'scale-by-scale'. In order to do that, we analyse scaling by using the local scaling exponent (LSE) given by the log-derivative of SFs:

$$\zeta_L^{(p)}(r) \equiv \frac{\mathrm{d}\log S_L^{(p)}(r)}{\mathrm{d}\log r}; \qquad \zeta_T^{(p)}(r) \equiv \frac{\mathrm{d}\log S_T^{(p)}(r)}{\mathrm{d}\log r}. \tag{3.1}$$
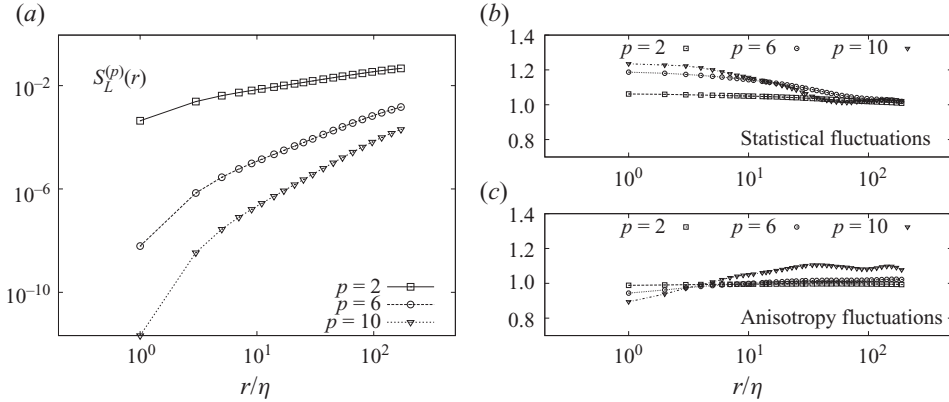
FIGURE 4. (*a*) Log–log plot of longitudinal ESFs, $S_L^{(p)}(r)$ for $p = 2, 6, 10$. (*b*) Estimate of the statistical fluctuations, obtained by plotting the ratio of $S_L^{(p)}(r)$ calculated over the whole statistics or over one half of it. (*c*) Estimate of the anisotropic fluctuations, $\langle[u_x(\boldsymbol{x} + r_x) - u_x(\boldsymbol{x})]^p\rangle/\langle[u_y(\boldsymbol{x} + r_y) - u_y(\boldsymbol{x})]^p\rangle$, for $p = 2, 6, 10$. The sum of the two error sources leads to error bars that are of the order of the symbol size in (*a*).

The advantage of the LSE is twofold. First, it allows for assessing statistical properties locally, removing large-order non-universal contributions coming from the overall prefactors in the SF. Second, and more importantly, it assesses scaling without the need for any fitting; in other words, it is just the outcome of a measure and it does not depend on an 'arbitrary' definition as the extension of the inertial range, in order to define the degree of intermittency. For instance, let us consider the scaling of the fourth-order longitudinal flatness. It is easy to see that it can be rewritten, independently of any scaling assumptions and for all separations r, as:

$$F_L^{(4)}(r) = \frac{S_L^{(4)}(r)}{(S_L^{(2)}(r))^2} = (S_L^{(2)}(r))^{\phi_L^{(4)}(r)}; \qquad \phi_L^{(4)}(r) = \frac{\zeta_L^{(4)}(r)}{\zeta_L^{(2)}(r)} - 2. \qquad (3.2)$$

In other words, the presence of intermittency, i.e. a non-trivial scale-dependent flatness behaviour, is directly measured by how much the ratio of the LSE, $\zeta_L^{(4)}(r)/\zeta_L^{(2)}(r)$, is different from its dimensional value, 2, scale-by-scale. Let us start to analyse the LSE for the longitudinal and transverse ESF. In figure 5 we show the LSE for $p = 2, 4, 6, 8$ and in figure 6 we show the LSE for $p = 10$. Let us first notice that longitudinal and transverse statistics have significantly different viscous cut-offs, with transverse fluctuations having the tendency to have less important viscous damping with respect to the longitudinal ones (Gotoh *et al.* 2002). This is an effect already present for low-order $p = 2$ (figure 5*c*) and therefore certainly induced, at least partially, by geometrical constraints as the ones discussed about (2.3). Beside this remark, let us also notice the small – in amplitude, but important in principle – difference in the scaling exponents between longitudinal and transverse fluctuations. Up to $p = 4$ the LSEs are almost coinciding, within error bars, in the range of scales $r/\eta \in [20:80]$. For larger orders we start to detect a difference, with the transverse being systematically below the longitudinal. This difference becomes significantly visible for $p = 10$ as shown separately in figure 6. Note that this statement is not the outcome of any fitting procedure, and what is shown in figures 5 and 6 is a measurement independent of any theoretical interpretation. On the other hand, in order to decide about the existence, and extension, of a 'power law' range needs some fitting. The value of
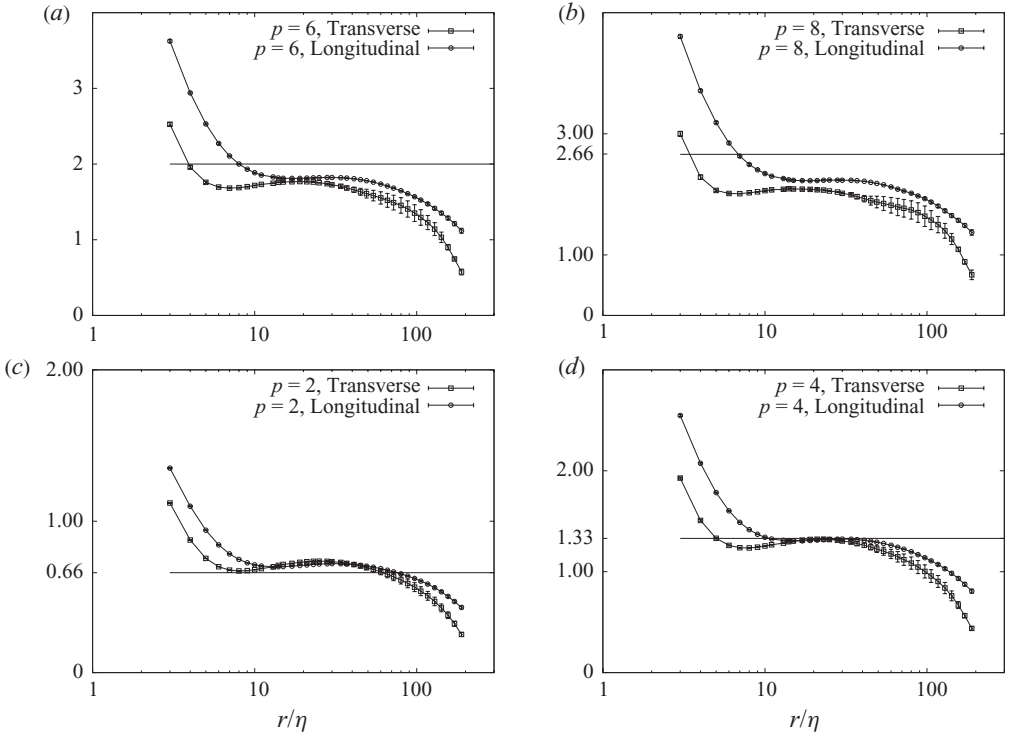
FIGURE 5. Local scaling exponents, $\zeta_L^{(p)}(r)$, $\zeta_T^{(p)}(r)$ of Eulerian longitudinal and transverse SFs for $p = 2, 4, 6, 8$. Error bars are obtained by estimating the residual anisotropy, given by the spread between measurements on different directions, $\boldsymbol{r}/r = \hat{x}, \hat{y}, \hat{z}$. Statistical error bars are smaller. The horizontal straight line corresponds to the Kolmogorov dimensional prediction, $\zeta^{(p)} = p/3$.
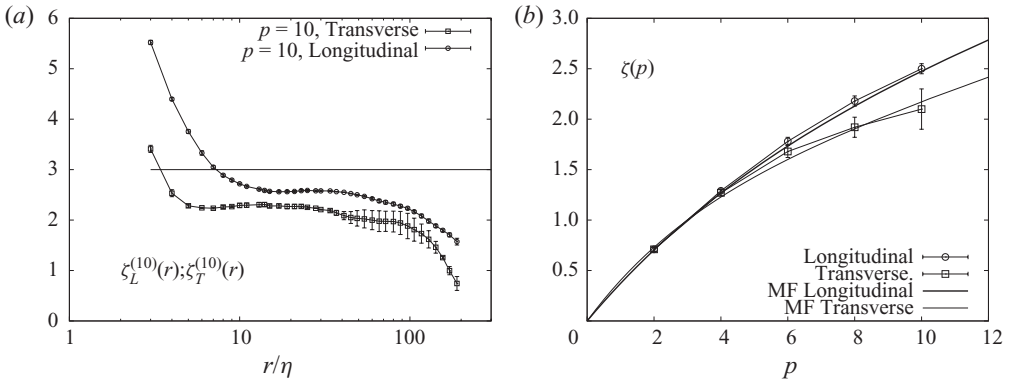

FIGURE 6. (a) Longitudinal and transverse local scaling exponents, the same as figure 5 but for $p = 10$. (b) Summary of the Eulerian scaling from table 1. The two solid lines represent a fit to the scaling exponents with two different multifractal spectrum $D_L(h)$ and $D_T(h)$ both having a log-Poisson statistics (Dubrulle 1994; She & Leveque 1994): $D_{L,T}(h) = (3(h - h^*))/(\log(\beta_{L,T})) \left[\log\left((3(h^* - h))/(d_{L,T}^* \log(\beta_{L,T}))\right) - 1\right] + 3 - d_{L,T}^*$. The only parameter we have hanged for the two data sets is $\beta_L = 0.6$ and $\beta_T = 0.4$, while we kept the highest singularity to be the same, $h^* = 1/9$. The fractal dimension of the highest singularity is then fixed by the requirement that $\zeta_L^{(3)} = \zeta_T^{(3)} = 1$, $d_{L,T}^* = (1 - 3h^*)/(1 - \beta_{L,T})$.

p	$\zeta_L^{(p)}$	$\zeta_T^{(p)}$	$\zeta_L^{(p)}$ [G02]	$\zeta_T^{(p)}$ [G02]	$\zeta_L^{(p)}/\zeta_L^{(3)}$	$\zeta_T^{(p)}/\zeta_T^{(3)}$
2	0.71 ± 0.02	0.71 ± 0.02	0.70 ± 0.01	0.71 ± 0.01	0.69 ± 0.005	0.71 ± 0.01
4	1.29 ± 0.03	1.27 ± 0.05	1.29 ± 0.03	1.26 ± 0.02	1.28 ± 0.01	1.26 ± 0.01
6	1.78 ± 0.04	1.68 ± 0.06	1.77 ± 0.04	1.67 ± 0.04	1.75 ± 0.01	1.68 ± 0.03
8	2.18 ± 0.05	1.92 ± 0.10	2.17 ± 0.07	1.93 ± 0.09	2.17 ± 0.03	1.98 ± 0.1
10	2.50 ± 0.06	2.10 ± 0.20	2.53 ± 0.09	2.08 ± 0.18	2.5 ± 0.05	2.25 ± 0.15

TABLE 1. Estimate of the global scaling exponents, out of the figures for the local scaling exponents (figures 5 and 6). The first and second columns refer to our numerics, the third and fourth to the data published in Gotoh *et al.* (2002) (G02) from a pseudo-spectral DNS at comparable Reynolds number. The last two columns correspond to the ESS estimate of our data, using the third-order longitudinal ESF as a reference for the scaling of $S_L^{(p)}(r)$ and using the third-order transverse ESF for the scaling of $S_T^{(p)}(r)$. Error bars are obtained by summing the uncertainty obtained from estimating the scaling in three different spatial directions (anisotropy contributions) and by changing the scaling range in the interval $r \in [10:100]\eta$, where the global exponent is evaluated.

the 'global' scaling exponent, $\zeta_L^{(p)}, \zeta_T^{(p)}$ would then be given by the average of the LSE in the region where they are close to constant. An error bar on the mean value can then be estimated on the basis of the oscillation induced by statistical and anisotropic effects in the fitting range and by the change as a function of the extension of the scaling range used to make the fit. Such a fitting procedure (detailed in the caption) leads to the summary for the 'global' Eulerian scaling exponents depicted in figure 6(*b*) and also summarized in table 1, where we compare our results with another pseudo-spectral DNS obtained with fully incompressible Navier–Stokes equations at comparable Reynolds numbers. From a theoretical point of view, we know that there are exact constraints that fix $\zeta_L^{(p)} = \zeta_T^{(p)}$ for $p = 2$ (for $p = 3$, a similar constraint fixes the scaling of third-order longitudinal SFs with mixed second-order transverse and first-order longitudinal increments). Moreover, there is no strong theoretical argument suggesting the possibility that for $p \geqslant 4$ one should expect a different scaling. Consequently, the results shown in figures 5 and 6 are not fully understood. Whether the difference between longitudinal and transverse ESF will shrink as one goes to higher Reynolds numbers remains to be investigated, and it is an important open question. The good news is that the value found in our numerics are in agreement with previous results (see table 1), making us confident that they are robust and are not dependent on compressibility. Even the relative scaling behaviour, obtained by plotting each SF versus the third-order one, a procedure known as extended self similarity (ESS) in the literature (Benzi *et al.* 1993, 1996), does not change much the above picture (not shown). In table 1 we also give the results of the LSE for both longitudinal and transverse ESF estimated by using ESS. Again a small spread between longitudinal and transverse is measured. Nevertheless, it is interesting to note that while the ESS procedure applied to longitudinal statistics reduces the error bars with respect the usual LSE considerably, for the transverse statistics there is no clear gain in adopting ESS. This may suggest the possibility that the different scaling behaviour detected between $S_L^{(p)}(r)$ and $S_T^{(p)}(r)$ may be due to different sub-leading corrections to the main leading scaling, contributing more to the transverse scaling than to the longitudinal. Due to the lack of any hints on the possible sub-leading correction we refrain here from entering into a fitting procedure with too many free parameters. The issue whether the difference in the LSE shown in figure 5
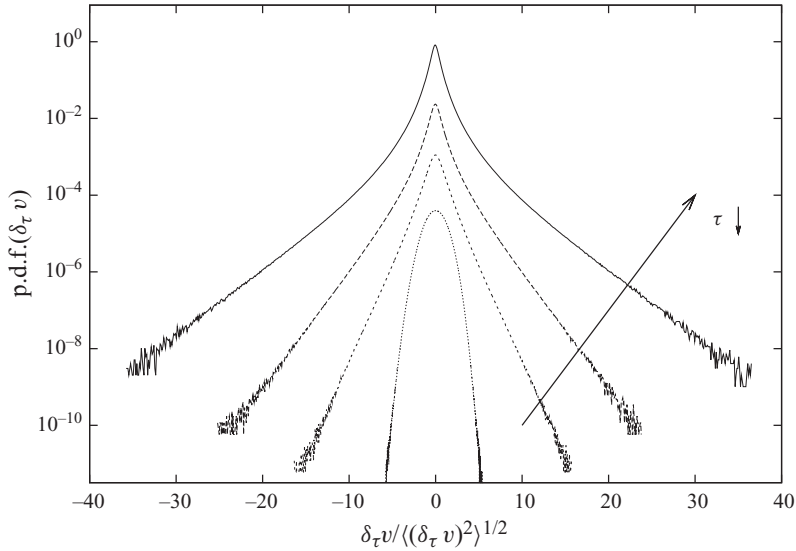
FIGURE 7. Lagrangian p.d.f. for a single component velocity increments along particle trajectories, over different time increments, $\tau \in [2\!:\!400]\tau_\eta$. Curves are shifted along the y-axis for presentation purposes.

is the signature of a true mismatch between the scaling properties of longitudinal and transverse fluctuations, or the result of a superposition of leading and sub-leading power laws with coinciding exponents between longitudinal and transverse but with different prefactors, remains open.

4. Intermittency and anomalous scaling in the Lagrangian inertial range

We now turn our attention to Lagrangian particles. As it is known, LSF shows very strong intermittency. In figure 7, we show the p.d.f. of $\delta_\tau v_i$ for different values of τ and averaging over the different velocity components: for small τ the probability density exhibits stretched exponential tails, as also measured experimentally in Mordant *et al.* (2001). Concerning the LSF, we show in figure 8 a first overview on a log–log scale for moments up to $p = 8$. From this figure we can already extract some conclusions. First, scaling in Lagrangian framework is not as good as the Eulerian one, as one can judge by the naked eye. This is a common feature of all Lagrangian statistics, and was already observed in many other experimental and numerical previous works.

The simplest explanation is that the finite Reynolds effects are more important in the Lagrangian domain: dimensional estimate gives for the Lagrangian inertial range extension the scaling $T_L/\tau_\eta \sim Re^{1/2}$, while in the Eulerian case we have $L/\eta \sim Re^{3/4}$. In the inset of figure 8, we show the importance of anisotropic fluctuations, by comparing the ratio between two LSF on two different components, $\mathscr{S}_x^{(p)}(\tau)/\mathscr{S}_y^{(p)}(\tau)$ for $p = 4, 8$. As one can see, the importance of anisotropic fluctuations is again of the order of 10 % at most, for the highest moments. Such corrections are of the order of the symbol size of the LSF averaged over the three components shown in the body of figure 8. Let us stress that anisotropic effects give also an hint on statistical error bars. Indeed, since our forcing is statistically isotropic, any anisotropic residual signal can be only due to limited statistical samples. The measured scaling in the Lagrangian domain does not allow for a systematic assessment on the local scaling exponents as
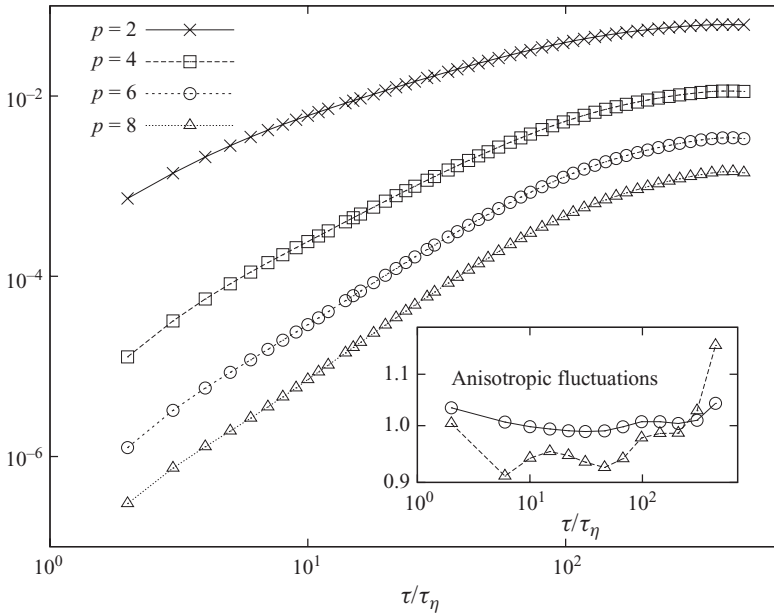
FIGURE 8. Log–log plot of LSF for $p = 2, 4, 6, 8$. Inset, estimate of the anisotropic statistical degree: ratio between two different components of LSF, $\langle (\delta_\tau v_x)^p \rangle / \langle (\delta_\tau v_y)^p \rangle$, for $p = 4$ (circles) and $p = 8$ (triangles).

done for the Eulerian field. Here, if one wishes to retain good local properties, it is necessary to resort to the ESS method, plotting the local scaling exponents relative to one moment versus a reference one (here taken the second order):

$$\chi^{(p)}(\tau) \equiv \frac{\mathrm{d} \log \mathscr{S}^{(p)}(\tau)}{\mathrm{d} \log \mathscr{S}^{(2)}(\tau)}, \tag{4.1}$$

which are related, in presence of pure power-law scaling, to the scaling exponents of the LSF defined from (1.2) by the obvious relation:

$$\chi^{(p)}(\tau) \sim const. = \xi^{(p)} / \xi^{(2)}. \tag{4.2}$$

Let us stress, nevertheless, that the importance of the local exponents (4.1) goes much beyond their interpretation as a simple proxy of the ratio between the SFs exponents (4.2). Indeed, they give a clear and simple way to assess the importance of intermittency in the Lagrangian domain as the only quantities entering in the scaling properties of Lagrangian hyper-flatness:

$$\mathscr{F}^{(p)}(\tau) = \frac{\mathscr{S}^{(2p)}(\tau)}{(\mathscr{S}^{(2)}(\tau))^2} = (\mathscr{S}^{(2)}(\tau))^{\chi^{(2p)}(\tau) - p/2}. \tag{4.3}$$

Again, here, the same comment made for the Eulerian case is in order: via the Lagrangian hyper-flatness (4.3) we are able to assess intermittency in a quantitative way, 'free of any fitting ambiguity', without having to assume power-law properties, by simply checking the difference between $\chi^{(2p)}(\tau)$ and $p/2$, scale-by-scale. In figure 9 we show the hyper-flatness local exponents for $p = 4, 6, 8, 10$. The scaling range extends up to more than one decade, for $\tau/\tau_\eta \in [20 : 300]$. As one can see, there are two remarkable facts. First, the Lagrangian scaling is much more intermittent then the Eulerian one, if measured in terms of deviations from the dimensional scaling given
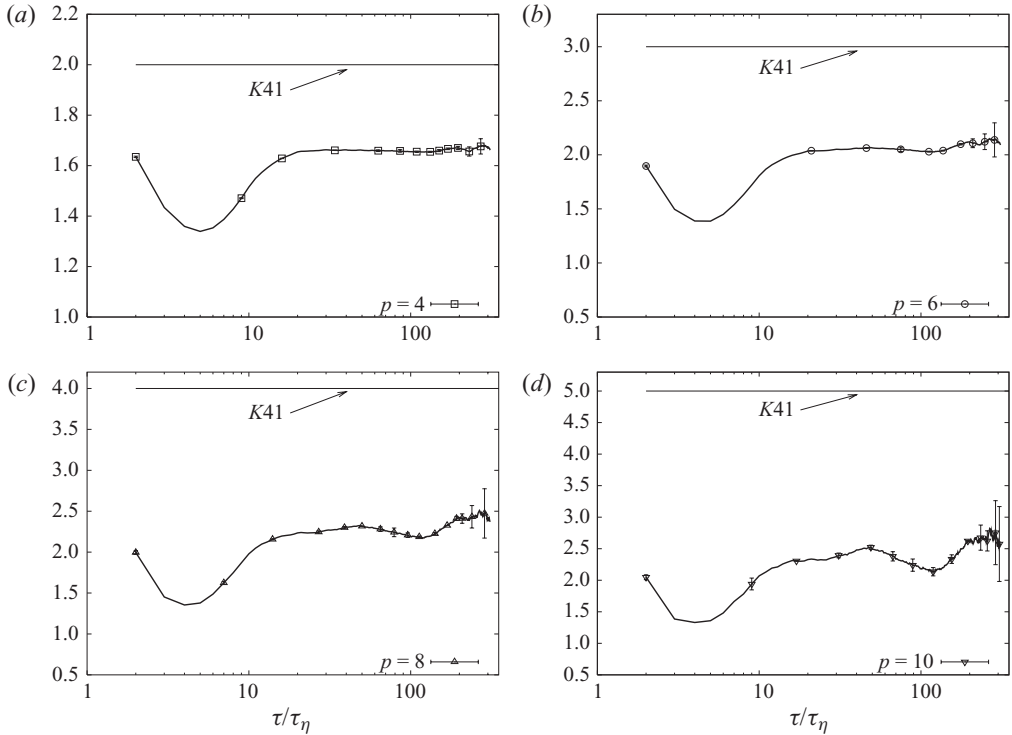
FIGURE 9. Lagrangian local scaling exponents for hyper-flatness, $\chi^{(p)}(\tau)$, for $p = 4, 6, 8, 10$. Notice the extremely good scaling behaviour for low moments, which deteriorates only mildly for $p = 6, 8$. Notice also the dip region close to the viscous time scales, an effect interpreted in terms of trapping into vortex filaments (Jimenez *et al.* 1993; Bec *et al.* 2006). The horizontal straight lines (K41) correspond to the dimensional Kolmogorov scaling $\chi^{(p)} = p/2$. Error bars are an estimate of the anisotropic effects and are obtained by comparing the measurements on three different velocity components.

by the Kolmogorov 1941 theory, $\chi(p) = p/2$. For example, for $p = 10$, we measure $\chi^{(10)} = 2.45 \pm 0.35$, which is 50 % off from the dimensional value $\chi^{(10)} = 5$. The second fact is the strong dip measured across the viscous scale, for time lags $\tau/\tau_\eta \in [1:10]$. This is similar to the Eulerian 'bottleneck' (Lohse 1994), while for the LSFs, this was observed first in Mazzitelli & Lohse (2004) and interpreted as being induced by the presence of small scale vortex filaments in Biferale *et al.* (2005) and Bec *et al.* (2006). The value of the Lagrangian exponents measured in our numerics in the inertial range are reported in table 2 and compared with previous measurements on other DNS or experiments. Let us stress 'that there are currently no other measurements of the higher-order LSFs with comparable statistics and Reynolds numbers as the one presented here'. A global fit in log–log of the scaling properties does not allow disentangling the inertial range from viscous–inertial contribution (affected by the dip visible for $\tau \sim \tau_\eta$) as they emerge from figure 9. This explains the slightly systematic underestimate of the scaling exponents from all previous studies, in comparison to those found here. The only data presented previously for $p = 8, 10$ at comparable Reynolds are those published in Xu *et al.* (2006), where the scaling properties are estimated very close, if not inside, the dip region, $\tau \in [3:6]\tau_\eta$. Similar uncertainty occurs with the data in Homann *et al.* (2007). The numerical data for $p = 8, 10$ presented in Mordant *et al.* (2006) also underestimate the value of the scaling properties with

$\chi^{(p)}$	$p = 4$	$p = 6$	$p = 8$	$p = 10$
Our numerics ($R_\lambda \sim 600$)	1.66 ± 0.02	2.10 ± 0.10	2.33 ± 0.17	2.45 ± 0.35
EXP1 ($R_\lambda \sim 800$)	1.47 ± 0.18	1.73 ± 0.25	1.92 ± 0.32	1.98 ± 0.38
EXP2 ($R_\lambda \in [500:1000]$)	1.56 ± 0.06	1.80 ± 0.20	—	—
DNS1 ($R_\lambda \sim 320$)	1.51 ± 0.04	1.76 ± 0.11	—	—
DNS2 ($R_\lambda \sim 75$)	1.56 ± 0.03	1.82 ± 0.08	1.92 ± 0.14	1.93 ± 0.3

TABLE 2. First row: summary of the local scaling exponents for Lagrangian statistics as extracted from our data shown in figure 9. Error bars are evaluated out of the anisotropic statistical degree, estimating the LSE out of the three different velocity components and by changing the fit range in the interval $\tau \in [20:200]$. Statistical fluctuations due to finite sampling are of the same order of anisotropic effects. The other rows correspond to other data available for high-order moments from both experiments at comparable Reynolds numbers and numerical works at smaller Reynolds numbers. EXP1 (Xu *et al.* 2006); EXP2 (Mordant *et al.* 2006); DNS1 (Homann *et al.* 2007); DNS2 (Mordant *et al.* 2006).

respect to our data. Probably, in this case, the low value of the Reynolds number ($R_\lambda \sim 75$) is such that the whole scaling region is dominated by the viscous dip. Considering all these pitfalls, we may conclude that when scaling properties are analyzed in the inertial range and where statistical fluctuations are not too high, there exists a good universality in Lagrangian statistics, as also tested quantitatively for $p = 4, 6$ in Biferale *et al.* (2008) and Arneodo *et al.* (2008). As for the universality of high-order moments, from $p = 8$ and up, we need to wait for other data with statistical properties and Reynolds number comparable with those of this study, to decide.

5. Multifractal: a link between Eulerian and Lagrangian statistics

Multifractals were introduced 25 years ago to explain deviations to the Kolmogorov scaling for Eulerian isotropic turbulent fluctuations (Parisi & Frisch 1985; see also Boffetta, Mazzino & Vulpiani 2008 for a recent review). The multifractal theory has since been extended to describe velocity gradients (Nelkin 1990; Benzi *et al.* 1991), multiscale velocity correlations (Meneveau & Chabra 1990; Belinicher *et al.* 1998) and fluctuations of the Kolmogorov viscous scale (Paladin & Vulpiani 1987; Frisch & Vergassola 1991; Meneveau 1996; Biferale 2008). Let us note that other attempts have been made to introduce fluctuations of the Kolmogorov scale in turbulence (L'vov & Procaccia 1996; Yakhot & Sreenivasan 2004, 2005); most of these predictions are either equivalent to or yield results almost indistinguishable from the multifractal approach given here.

In principle, one is free to develop different, uncorrelated, multifractal descriptions for Eulerian and Lagrangian quantities. On the other hand, in reality, Eulerian and Lagrangian measurements are of course intimately linked. One is therefore naturally tempted to develop a 'unified' multifractal description, able to describe both temporal and spatial fluctuations (Borgas 1993; Boffetta *et al.* 2002). In the following we describe such a development starting from the inertial range (where we can test it against our data) and extending into the viscous range.

5.1. *Inertial range*

Concerning Eulerian multifractal theory in the inertial range, the idea goes back to Parisi & Frisch (1985). Suppose we have different velocity fluctuations with

different local Hölder exponents, $\delta_r u \sim r^h$, for scale separation in the inertial range. Suppose that the set where the velocity field has an h-exponent is a fractal set with dimension $D(h)$. Then the ESF can be easily rewritten as an ensemble average over all possible h-fluctuations: $\langle (\delta_r u)^p \rangle = \int_h \mathrm{d}h\, r^{hp} r^{3-D(h)} \sim r^{\zeta^{(p)}}$, where the factor $r^{3-D(h)}$ gives the probability to fall on the fractal set with h-exponent at scale r, and where we have neglected, for the moment, any difference between longitudinal and transverse scalings, calling the generic Eulerian increment, $\delta_r u$. The last passage is obtained in the saddle point limit $r \to 0$:

$$\zeta^{(p)} = \min_h \left(hp + 3 - D(h) \right). \tag{5.1}$$

It is easy to imagine many different possible $D(h)$ distributions – built in terms of a random cascade – leading to a set of exponents $\zeta^{(p)}$ close to those measured. In a previous section, we had shown that both our numerics and previous DNS suggest that it is possible to have different scaling exponents for longitudinal or transverse SF. Therefore, we must allow two different sets of fractal dimensions, $D_L(h)$ and $D_T(h)$ describing the statistics. For example, in figure 6(b) we show the result of the saddle point (5.1) obtained with two different fractal spectra, tuned to fit the empirical scaling exponents as found from our numerics (see caption for details).

One possible way to simply link the Eulerian and Lagrangian statistics is to follow the ideas of Borgas (1993). As far as scaling is concerned, in three-dimensional turbulence we may imagine that the only relevant time in the inertial range is the local eddy turnover time:

$$\tau(r) \sim r/(\delta_r u) \sim r^{1-h}. \tag{5.2}$$

Then, we may assume that the Lagrangian velocity increment over a time lag τ must be of the order of the corresponding Eulerian velocity increments over a scale r with r and τ connected by (5.2):

$$\delta_\tau v \sim \delta_r u, \qquad \tau \sim r^{1-h},$$

where we neglect large scale $O(1)$ dimensional quantities connected to the root-mean-square total kinetic energy and to the box size. By using only this simple statement one is able to link now the LSF to the ESF, writing:

$$\langle (\delta_\tau v)^p \rangle = \int_h \mathrm{d}h\, \tau^{hp/(1-h)} \tau^{(3-D(h))/(1-h)} \sim \tau^{\xi^{(p)}}, \tag{5.3}$$

with now the Lagrangian exponents given by the saddle point estimate (Boffetta *et al.* 2002):

$$\xi^{(p)} = \min_h \left(\frac{hp + 3 - D(h)}{1 - h} \right). \tag{5.4}$$

It is important to notice that via the translation factor (5.2) we obtain two different sets of Lagrangian and Eulerian exponents but given by the same $D(h)$ curve. The exponents are different because the local eddy turnover is itself a fluctuation quantity, depending on the local scaling exponent, h.

Once given the $D(h)$, extracted from a fitting of the Eulerian statistics, it is tempting to use it as an input in (5.4) to get a prediction with 'no free' parameters for the Lagrangian scaling. Indeed, because the Eulerian statistics are different depending if one takes longitudinal or transverse fluctuations, and because it is very natural to think that during the Lagrangian evolution both fluctuations are felt, one may
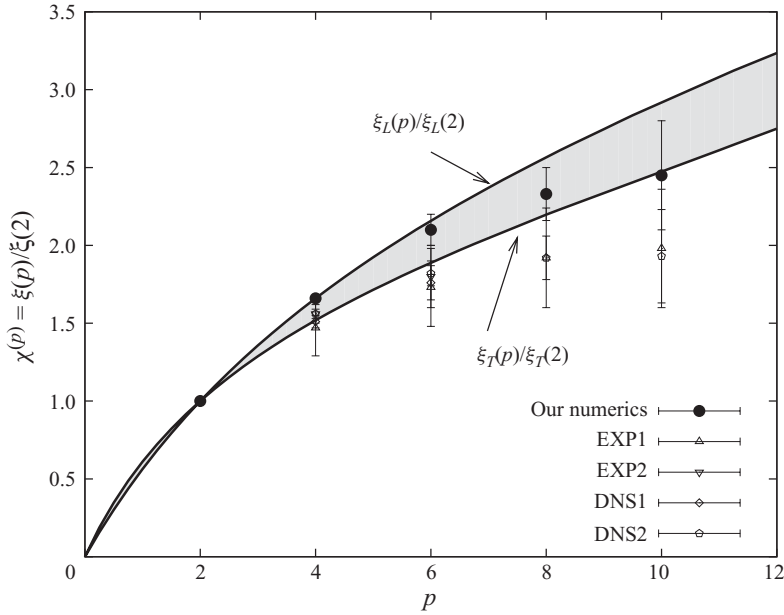
FIGURE 10. Summary of the Lagrangian scaling exponents, $\chi(p) = \xi(p)/\xi(2)$ (circles), as measured in the inertial range in our numerics, together with the prediction obtained from the Eulerian statistics by using the bridge relation either with the longitudinal Eulerian statistics (upper limit of the shadowed area) or with the transverse one (lower limit of the shadowed area). Previous measurement of Lagrangian scaling exponents are also shown (see table 2).

imagine to get two different predictions for the Lagrangian exponents:

$$\xi_{L,T}^{(p)} = \min_h \left(\frac{hp + 3 - D_{L,T}(h)}{1 - h} \right); \tag{5.5}$$

depending which Eulerian statistics one uses, $D_L(h)$ or $D_T(h)$. In figure 10 we show the comparison between the empirical Lagrangian exponents as extracted from our numerics (see table 2 and figure 9) and the two predictions one get using the longitudinal, $D_L(h)$ or transverse, $D_T(h)$, expression in (5.5). As one can see the agreement is good, indicating that the simple, but non-trivial, bridge relation (5.2) is working well and capturing the main scaling properties of both Eulerian and Lagrangian statistics. This is the first time the Lagrangian–Eulerian bridge relation is probed to such high level of accuracy, and it must be considered our most important result. Previous Lagrangian data for high orders, on the other hand, deviate from the MF prediction. We interpret this deviation as an effect induced by a global log–log fit of the scaling properties, contaminated by viscous corrections close to dip observed at $\tau_\eta \sim O(1)$, which tend to lower the value of the exponent if not disentangled properly, as discussed in §(4).

From figure 10 one may see that only for the highest-order $p = 10$, one starts to see a trend deviating from what is predicted by the Eulerian–Lagrangian bridge relation, although it is still within our error bars. Whether this deviation at high orders is the signature of very intense Lagrangian fluctuations bringing new information beyond that collected by (5.2) or not is an open and interesting question. However, it is not possible to address this question until new empirical and numerical data allow us to access these higher-order statistics for both Eulerian and Lagrangian domains.

5.2. *Dissipative effects*

The ability to assess Lagrangian data both numerically and experimentally in the inertial range has also opened the way to investigate dissipative and sub-dissipative time scales. For Eulerian statistics it is very difficult to have reliable data at scales smaller then η, due to either limitations induced by the experimental probe size or limitations of the numerical resolution (see Yamazaki, Ishihara & Kaneda 2002; Schumacher 2007; Schumacher, Sreenivasan & Yakhot 2007; Watanabe & Gotoh 2007 for recent DNS meant to address this issue). For Lagrangian quantities, the development of non-intrusive experimental techniques (mainly based on fast camera Toschi & Bodenschatz 2009) and the advancements of numerical algorithms to track particles have allowed for assessing time fluctuations of the order of $0.1\tau_\eta$, even at high Reynolds numbers. As a result, we may now pose new question about the statistical fluctuations for $\tau \sim \tau_\eta$ or smaller. Recently, a lot of attention has been given to the dip region visible in the local Lagrangian scaling exponents shown in numerical and experimental studies (Arneodo *et al.* 2008). In the last twenty years, a great deal work has been done to include viscous fluctuations in the multifractal theory, initially for Eulerian statistics (Paladin & Vulpiani 1987; Nelkin 1990; Benzi *et al.* 1991; Frisch & Vergassola 1991; Meneveau 1996), and more recently also for Lagrangian statistics (Chevillard *et al.* 2003; Biferale *et al.* 2004). Unfortunately, our numerics do not allow for a direct quantitative probe of scales deep in the viscous region, because of the numerical dissipative nature of the FLASH code. So, we limit our discussion here to a theoretical one: specifically, what are the predictions of the MF for scaling within the dissipative regime? According to the MF theory, the viscous scale is not a fixed homogeneous quantity, but fluctuates wildly due to intermittency. Moreover, viscous and inertial fluctuations are linked by the requirement that viscous effects happen when the local Reynolds number becomes $O(1)$):

$$\frac{\delta_\eta u \, \eta}{\nu} \sim O(1); \quad \eta^{1+h} \sim \nu; \quad \eta(h) \sim Re^{-1/(1+h)}, \tag{5.6}$$

where we have taken for simplicity, $L = 1$, $U_0 = 1$ and $\nu = Re^{-1}$. Using the bridge relation (5.2), we may immediately find out the equivalent fluctuating relationship for the Kolmogorov dissipative time (Chevillard *et al.* 2003; Biferale *et al.* 2004):

$$\tau_\eta(h) \sim \eta^{1-h} \sim Re^{(h-1)/(1+h)}. \tag{5.7}$$

Taking this into account, one may use a Batchelor–Meneveau like parametrization for velocity increments for all time lags, including the fluctuating viscous time (Sirovich, Smith & Yakhot 1994; Meneveau 1996; Chevillard *et al.* 2003; Arneodo *et al.* 2008):

$$\delta_\tau v = V_0 \frac{\tau}{T_L} \left[\left(\frac{\tau}{T_L} \right)^\alpha + \left(\frac{\tau_\eta(h)}{T_L} \right)^\alpha \right]^{(2h-1)/(\alpha(1-h))}, \tag{5.8}$$

where α is a free parameter controlling the crossover around $\tau \sim \tau_\eta$ and V_0 is the root-mean-square large-scale velocity. In order to get a prediction for the behaviour of the LSF we need also to introduce dissipative effects in the MF probability. This can be done as follows:

$$P_h(\tau, \tau_\eta) = \mathscr{Z}^{-1}(\tau) \left[\left(\frac{\tau}{T_L} \right)^\alpha + \left(\frac{\tau_\eta(h)}{T_L} \right)^\alpha \right]^{(3-D(h))/(\alpha(1-h))}, \tag{5.9}$$

where $\mathscr{Z}$ is a normalizing function and $D(h)$ is the fractal dimension of the support of the exponents h. At this point, given the Reynolds number, we are left with two
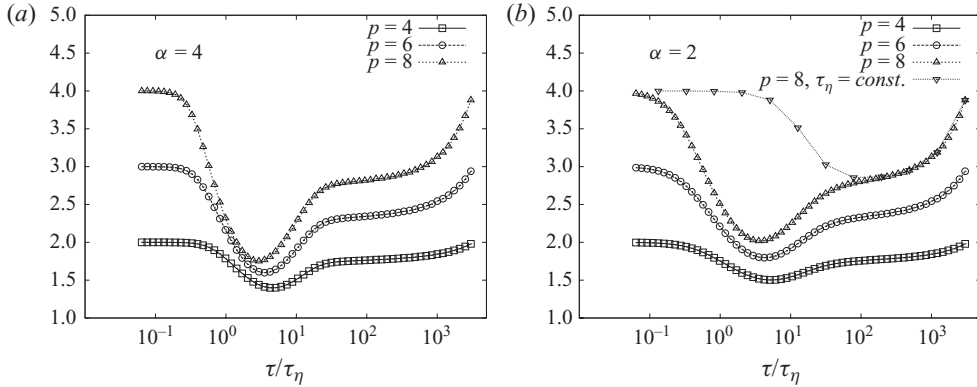
FIGURE 11. Results for the local Lagrangian exponents, $\chi^{(p)}(\tau)$ as obtained from the finite Reynolds multifractal formula (5.8)–(5.10) for a given Reynolds number and $p = 4, 6, 8$, with two choices of the free parameter, α, for differing dip regions. (a) $\alpha = 4$; (b) $\alpha = 2$, and $\chi^{(8)}(\tau)$ obtained from the same multifractal formula but keeping fixed the dissipative time scales, $\tau_\eta(h) = const.$, where the dip region disappears.

parameters (α and a multiplicative constant in the definition of τ_η). In order to compute the LSF at all time lags, one needs to integrate the expression (5.8) with the weight given by (5.9) over all possible h-values:

$$\langle(\delta_\tau v)^p\rangle \sim \int_{h_{min}}^{h_{max}} dh\, P_h(\tau)[\delta_\tau v(h)]^p. \tag{5.10}$$

Clearly, the above picture goes back to the inertial values when we have $\tau/T_L \to 0$ and $\tau \gg \tau_\eta$, i.e. when we can neglect viscous effects and we can perform the saddle point estimate. First, let us see what the qualitative impact of changing the free parameters is (see 5.8). In figure 11 we show the results for $\chi^{(p)}(\tau)$ as obtained from the global MF description (5.10) for $p = 4, 6, 8$ with a fixed $D(h)$ by changing the free parameter $\alpha = 4$ (figure 11a) or $\alpha = 2$ (figure 11b). From this figure we learn two things. The MF description is very close to the real data, compared with figure 9(a). In particular, the dip present in the data is also captured by the MF (Arneodo *et al.* 2008). Moreover, by changing the free parameter α one may deplete or enhance the dip intensity, as can be seen comparing figures 11(a) and 11(b). We may also note that the dip region is entirely due to the presence of the fluctuating viscous cut-off, $\tau_\eta(h)$, as can be seen in figure 11(b), where the same data for $p = 8$ but with a fixed τ_η are plotted and the dip has disappeared.

Second, from figure 11 one sees that for any finite Reynolds numbers, there are corrections to scaling induced by the large time lags T_L; as a consequence, in the inertial range the local exponents are not exactly constant. In order to give a qualitative assessment of the importance of this finite Reynolds correction as described by (5.8), we plot in figure 12(a) the values of $\chi^{(4)}(\tau)$ for three different Reynolds numbers. As one can see, at increasing Reynolds, the curves in the inertial range become flatter and flatter, as they must do.

Another interesting issue is connected to finite Reynolds effects. As opposed to the limit of infinite Reynolds number, for any finite Reynolds, the whole support of $D(h)$ will play a role in the integration (5.10): for larger τ/T_L the saddle point estimate (5.4) becomes less and less accurate. As a result, the whole shape of the $D(h)$ curve becomes important for any order. Indeed, the typical $D(h)$ curve from any MF theory
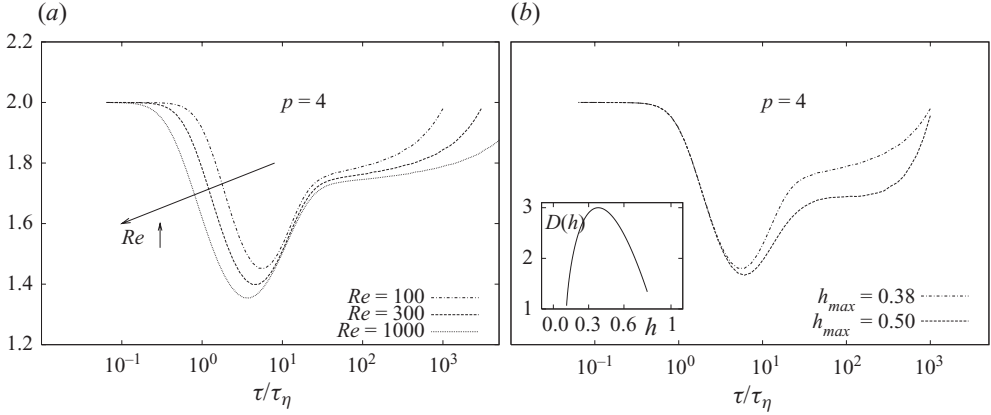
FIGURE 12. (*a*) Reynolds effects on the local exponents predicted from the MF interpolation formula (5.8)–(5.10), we kept fixed everything except the Reynolds numbers. (*b*) Sensitivity to the whole shape of the $D(h)$ curve of the $\chi^{(4)}(\tau)$ as predicted from the MF interpolation formula. We show two cases. One case is obtained integrating only on fluctuations in the left region of the $D(h)$ curve with respect to its peak, $h \in [h_{min}, h_{max}]$, with $h_{max} = h_{peak} = 0.38$; the second case also considers smoother fluctuations up to $h_{max} = 0.5$. The typical log-Poisson shape of the $D(h)$ used is depicted in the inset.

is a convex function like the one used to fit the Eulerian longitudinal exponents depicted in the inset of figure 12(*b*). The left part of $D(h)$ curve, with $h \in [h_{min}, h_{peak}]$, is connected to the positive order of the ESFs (Frisch 1995). The right-hand side, $h \in [h_{peak}, h_{max}]$, is connected to negative moments. Negative moments are generally ill-defined and one needs to use inverse statistics to assess the right part of the $D(h)$ curve (Biferale *et al.* 1999; Jensen 1999). Because of that, we have a good control only on the left-hand side, where most of the previous experimental and numerical studies focused. The extension of the integration in (5.10) over the h-value on the right of the peak of $D(h)$ is therefore not based on solid experimental or numerical basis. The extension to the right part of a given functional form for $D(h)$ (log-Poisson, log-normal, etc.), obtained by fitting only positive moments of SFs (Chevillard *et al.* 2003) is therefore arbitrary.

In figure (12*b*) we show the dependence of the final expression (5.10) from the extension of the integration over the h-range. As one can see, the inclusion of h-value falling on the right of the peak gives an important contribution to the behaviour of the local slopes for $\tau \sim T_L$, confirming the importance of the whole $D(h)$ if one wants to control the finite-Reynolds corrections to the saddle point estimate (5.4). For a more detailed investigation of the property of the multifractal formulation (5.10) also compared with other DNS and experimental results, the reader can consult the recent collection of data published in Arneodo *et al.* (2008).

6. Conclusions

We have reported new Eulerian and Lagrangian statistics from high-resolution numerical simulations of homogeneous, isotropic weakly compressible turbulence. The Reynolds number at the Taylor microscale is estimated to be around 600. We have analyzed, for the first time, Lagrangian intermittency 'scale-by-scale' up to moments of order 10, at large Reynolds numbers. The four main results we have presented are as follows: (i) Eulerian longitudinal and transverse statistics have slightly

different scaling properties, in agreement with previous incompressible DNS data at comparable resolution. (ii) Lagrangian statistics are more intermittent than Eulerian ones percentagewise with respect to the observed deviations from dimensional scaling; its quantitative value can be captured by using a simple multifractal bridge relation. (iii) In order to correctly assess Lagrangian scaling properties it is necessary to make a scale-by-scale analysis, in order to disentangle the dip region close to viscous scales from the inertial range interval. A lack of such analysis may lead to an underestimate of the Lagrangian scaling exponents, because of the strong intermittency of the dip interval, dominated by viscous effects. (iv) Multifractal phenomenology is able to describe dissipative effects, inertial range fluctuations and large-scale corrections in a unified way (Chevillard *et al.* 2003; Arneodo *et al.* 2008). Here in figures 11 and 12 we have shown the importance of viscous scale fluctuations, finite Reynolds effects and the $D(h)$ shape on the local scaling exponents, 'scale-by-scale'.

This study leaves open a few important questions. First, we need to wait for higher Reynolds numbers data, in a highly isotropic ensemble, in order to resolve the riddle about longitudinal versus transverse Eulerian fluctuations. Second, we also need to collect data with higher-order Lagrangian statistics to understand whether the Eulerian–Lagrangian bridge relation remains valid for higher moments. Third, it is important to improve experimental and numerical accuracy in order to measure small-scale and small-time fluctuations, where highly non-trivial physics exists as shown by the strong enhancement of local intermittency in the dip region $\tau \in [1:10]\tau_\eta$ (Arneodo *et al.* 2008). Such strong enhancement of fluctuations around the viscous scale is due to local fluctuations of the dissipative cut-off, which reflects the existence of different viscous effects for different moments and different correlation functions (Frisch & Vergassola 1991; L'vov & Procaccia 1996; Yakhot & Sreenivasan 2004). It is well described, within the multifractal theory, by the relation (5.6), as shown by the fact that the dip region disappears by removing the viscous fluctuations in (5.8) and (5.9), see the right-hand side of figure 11. This effect is probably the greatest barrier to overcome in both stochastic modelling (Sawford 2001) and theory of Lagrangian turbulence (Zybin *et al.* 2008; V. Yakhot 2009, private communication).

REFERENCES

ALEXAKIS, A., CALDER, A. C., HEGER, A., BROWN, E. F., DURSI. L. J., TRURAN. J. W., ROSNER, R., LAMB, D. Q., TIMMES, F. X., FRYXELL, B., ZINGALE, M., RICKER, P. M. & OLSON, K. 2004 On heavy element enrichment in classical novae. *Astrophys. J.* **602**, 931.

ARNEODO, A., BAUDET, C., BELIN, F., BENZI, R., CASTAING, B., CHABAUD, B., CHAVARRIA, R., CILIBERTO, S., CAMUSSI, R., CHILLA, F., DUBRULLE, B., GAGNE, Y., HEBRAL, B., HERWEIJER, J., MARCHAND, M., MAURER, J., MUZY, J. F., NAERT, A., NOULLEZ, A., PEINKE, J., ROUX, F., TABELING, P., VAN DE WATER, W. & WILLAIME, H. 1996 Structure functions in turbulence, in various flow configurations, at Reynolds number between 30 and 5000, using extended self-similarity. *Europhys. Lett.* **34**, 411.

ARNEODO, A., BENZI, R., BERG, J., BIFERALE, L., BODENSCHATZ, E., BUSSE, A., CALZAVARINI, E., CASTAING, B., CENCINI, M., CHEVILLARD, L., FISHER, R. T., GRAUER, R., HOMANN, H., LAMB, D., LANOTTE, A. S., LÉVÊQUE, E., LUTHI, B., MANN, J., MORDANT, N., MULLER, W.-C., OTT, S.,

OUELLETTE, N. T., PINTON, J.-F., POPE, S. B., ROUX, S. G., TOSCHI, F., XU, H. & YEUNG, P. K. 2008 Universal intermittent properties of particle trajectories in highly turbulent flows. *Phys. Rev. Lett.* **100**, 254504.

ARNETT, D., FRYXELL, B. & MUELLER, E. 1989 Instabilities and nonradial motion in SN 1987A. *Astrophys. J. Lett.* **341**, L63.

BEC, J., BIFERALE, L., CENCINI, M., LANOTTE, A. & TOSCHI, F. 2006 Effects of vortex filaments on the velocity of tracers and heavy particle in turbulence. *Phys. Fluids* **18**, 081702.

BELINICHER, V. I., L'VOV, V., POMYALOV, A. & PROCACCIA, I. 1998 Computing the scaling exponents in fluid turbulence from first principles: demonstration of multiscaling. *J. Stat. Phys.* **93**, 797–832.

BENZI, R., BIFERALE, L., CALZAVARINI, E., LOHSE, D. & TOSCHI, F. 2009 Velocity gradients statistics along particle trajectories in turbulent flows: the refined similarity hypothesis in the Lagrangian frame. *Phys. Rev.* E **80**, 066318.

BENZI, R., BIFERALE, L., CILIBERTO, S., STRUGLIA, M. V., TRIPICCIONE, R. 1996 Generalized scaling in fully developed turbulence. *Physica* D **96**, 162.

BENZI, R., BIFERALE, L., FISHER, R., KADANOFF, L., LAMB, D. & TOSCHI, F. 2008 Intermittency and universality in fully developed inviscid and weakly compressible turbulent flows. *Phys. Rev. Lett.* **100**, 234503.

BENZI, R., BIFERALE, L., PALADIN, G., VULPIANI, A. & VERGASSOLA, M. 1991 Multifractality in the statistics of the velocity gradients in turbulence. *Phys. Rev. Lett.* **67**, 2299.

BENZI, R., CILIBERTO, S., BAUDET, C., MASSAIOLI, F. & SUCCI, S. 1993 Extended self-similarity in turbulent flows. *Phys. Rev.* E **48**, R29.

BERG, J., LUTHI, B., MANN, J. & OTT, S. 2006 Backwards and forwards relative dispersion in turbulent flow: an experimental investigation. *Phys. Rev.* E **74**, 016304.

BERG, J., OTT, S., MANN, J. & LUTHI, B. 2009 Lagrangian structure functions in a turbulent flow at intermediate Reynolds number. *Phys. Rev.* E **80**, 026316.

BIFERALE, L. 2008 A note on the fluctuation of dissipative scale in turbulence. *Phys. Fluids* **20**, 031703.

BIFERALE, L., BODENSCHATZ, E., CENCINI, M., LANOTTE, A., OUELLETTE, N., TOSCHI, F. & XU, H. 2008 Lagrangian structure functions in turbulence: a quantitative comparison between experiment and direct numerical simulation. *Phys. Fluids* **20**, 065103.

BIFERALE, L., BOFFETTA, G., CELANI, A., DEVENISH, B. J., LANOTTE, A. & TOSCHI, F. 2004 Multifractal statistics of Lagrangian velocity and acceleration in turbulence. *Phys. Rev. Lett.* **93**, 064502.

BIFERALE, L., BOFFETTA, G., CELANI, A., LANOTTE, A. & TOSCHI, F. 2005 Particle trapping in three-dimensional fully developed turbulence. *Phys. Fluids* **17**, 021701.

BIFERALE, L., CENCINI, M., VERGNI, D. & VULPIANI, A. 1999 Exit time of turbulent signals: a way to detect the intermediate dissipative range. *Phys. Rev.* E **60**, R6295.

BIFERALE, L. & PROCACCIA, I. 2005 Anisotropy in turbulent flows and in turbulent transport. *Phys. Rep.* **414**, 43.

BOFFETTA, G., DE LILLO, F. & MUSACCHIO, M. 2002 Lagrangian statistics and temporal intermittency in a shell model of turbulence. *Phys. Rev.* E **66**, 066307.

BOFFETTA, G., MAZZINO, A. & VULPIANI, A. 2008 Twenty-five years of multifractals in fully developed turbulence: a tribute to Giovanni Paladin. *J. Phys.* A **41**, 363001.

BORATAV, O. & PELZ, R. 1997 Structures and structure functions in the inertial range of turbulence. *Phys. Fluids* **9**, 1400.

BORGAS, M. S. 1993 The multifractal Lagrangian nature of turbulence. *Phil. Trans. R. Soc.* A **342**, 379.

BOURGOIN, M., OUELLETTE, N., XU, H., BERG, J. & BODENSCHATZ, E. 2006 The role of pair dispersion in turbulent flow. *Science* **311**, 835.

CALDER, A. C., FRYXELL, B., PLEWA, T., ROSNER, R., DURSI, L. J., WEIRS, V. G., DUPONT, T., ROBEY, H. F., KANE, J. O., REMINGTON, B. A., DRAKE, R. P., DIMONTE, G., ZINGALE, M., TIMMES, F. X., OLSON, K., RICKER, P., MAC NEICE P. & TUFO, H. M. 2002 On validating an astrophysical simulation code. *Astrophys. J. Suppl.* **143**, 201.

CHEN, S., SREENIVASAN, K. R. & NELKIN, M. 1997 Inertial range scalings of dissipation and enstrophy in isotropic turbulence. *Phys. Rev. Lett.* **79**, 2253.

CHEVILLARD, L., ROUX, S,. LÉVÊQUE, E., MORDANT, N., PINTON, J.-F. & ARNEODO, A. 2003 Lagrangian velocity statistics in turbulent flows: effects of dissipation. *Phys. Rev. Lett.* **91**, 214502.

COLELLA, P. & WOODWARD, P. R. 1984 The piecewise parabolic method (PPM) for gas-dynamical simulations. *J. Comput. Phys.* **54**, 174.

DHRUVA, B., TSUJI, Y. & SREENIVASAN, K. R. 1997 Transverse structure functions in high-Reynolds-number turbulence. *Phys. Rev.* E **56**, R4928.

DUBRULLE, B. 1994 Intermittency in fully developed turbulence: log-Poisson statistics and generalized scale covariance. *Phys. Rev. Lett.* **73**, 959.

ESWARAN, V. & POPE, S. B. 1988 An examination of forcing in direct numerical simulations of turbulence. *Comput. Fluids* **16**, 257.

FISHER, R. T., KADANOFF, L. P., LAMB, D. Q., DUBEY, A., PLEWA, T., CALDER, A., CATTANEO, F., CONSTANTIN, P., FOSTER, I., PAPKA, M. E., ABARZHI, S. I., ASIDA, S. M., RICH, P. M., GLENDENING, C. C., ANTYPAS, K., SHEELER, D. J., REID, L. B., GALLAGHER, B. & NEEDHAM, S. G. 2007 Terascale turbulence computation on BG/L using the FLASH3 code. *IBM J. Res. Dev.* **52**, 127.

FRISCH, U. 1995 *Turbulence: The Legacy of A. N. Kolmogorov.* Cambridge University Press.

FRISCH, U. & VERGASSOLA, M. 1991 A prediction of the multifractal model: the intermediate dissipation range. *Europhys. Lett.* **14**, 439.

GOTOH, T., FUKAYAMA, D. & NAKANO, T. 2002 Velocity field statistics in homogeneous steady turbulence obtained using a high-resolution direct numerical simulation. *Phys. Fluids* **14**, 1065.

HE, G., CHEN, S., KRAICHNAN, R. H., ZHANG, R. & ZHOU, Y. 1998 Statistics of dissipation and enstrophy induced by localized vortices. *Phys Rev. Lett.* **81**, 4636.

HILL, R. 2001 Equations relating structure functions of all orders. *J. Fluid Mech.* **434**, 379.

HOMANN, H., GRAUER, R., BUSSE, A. & MUELLER, W. 2007 Lagrangian statistics of Navier–Stokes and MHD turbulence. *J. Plasma Phys.* **73**, 821.

HOMANN, H., KAMPS, O., FRIEDRICH, R. & GRAUER, R. 2009 Bridging from Eulerian to Lagrangian statistics in 3D hydro- and magnetohydrodynamic turbulent flows. *New J. Phys.* **11**, 073020.

ISHIHARA, T., GOTOH, T. & KANEDA, Y. 2009 Study of high-Reynolds Number isotropic turbulence by direct numerical simulation. *Annu. Rev. Fluid Mech.* **41**, 165.

JENSEN, M. H. 1999 Multiscaling and structure functions in turbulence: an alternative approach. *Phys. Rev. Lett.* **83**, 76.

JIMENEZ, J., WRAY, A. A., SAFFMAN, P. G. & ROGALLO, R. S. 1993 The structure of intense vorticity in isotropic turbulence. *J. Fluid Mech.* **255**, 65.

KANE, J. O., ROBEY, H. F., REMINGTON, B. A., DRAKE, R. P., KNAUER, J., RYUTOV, D. D., LOUIS, H., TEYSSIER, R., HURRICANE O., ARNETT, D., ROSNER, R. & CALDER A. 2001 Interface imprinting by a rippled shock using an intense laser. *Phys. Rev.* E **63**, 055401.

LA PORTA, A., VOTH, G. A., CRAWFORD, A. M., ALEXANDER, J. & BODENSCHATZ, E. 2001 Fluid particle accelerations in fully developed turbulence. *Nature* **409**, 1017.

LOHSE, D. 1994 Crossover from high to low-Reynolds-number turbulence. *Phys. Rev. Lett.* **73**, 3223.

LUETHI, B., TSINOBER, A. & KINZELBACH, W. 2005 Lagrangian measurement of vorticity dynamics in turbulent flow. *J. Fluid Mech.* **528**, 87.

L'VOV, V. S. & PROCACCIA, I. 1996 Viscous lengths in hydrodynamic turbulence are anomalous scaling functions. *Phys. Rev. Lett.* **77**, 3541.

MAZZITELLI, I. & LOHSE, D. 2004 Lagrangian statistics for fluid particles and bubbles in turbulence. *New J. Phys.* **6**, 203.

MENEVEAU, C. 1996 Transition between viscous and inertial-range scaling of turbulence structure functions. *Phys. Rev.* E **54**, 3657.

MENEVEAU, C. & CHABRA, A. 1990 Two-poi statistics of multifractal measures. *Physica* A **164**, 564.

MORDANT, N., LÉVÊQUE, E. & PINTON, J.-F. 2006 Experimental and numerical study of Lagrangian dynamics of high Reynolds turbulence. *New J. Phys.* **6**, 116.

MORDANT, N., METZ, P., MICHEL, O. & PINTON, J.-F., 2001 Measurement of Lagrangian velocity in fully developed turbulence. *Phys. Rev. Lett.* **87**, 214501.

NELKIN, M. 1990 Multifractal scaling of velocity derivatives in turbulence. *Phys. Rev.* A **42**, 7226.

OTT, S. & MANN, J. 2000 An experimental investigation of the relative diffusion of particle pairs in three- dimensional turbulent flow. *J. Fluid Mech.* **422**, 207.

PALADIN, G. & VULPIANI, A. 1987 Degrees of freedom of turbulence. *Phys. Rev.* A **35**, R1971.

PARISI, G. & FRISCH, U. 1985 In *Turbulence and Predictability in Geophysical Fluid Dynamics and Climate Dynamics*. Proceedings of the Enrico Fermi School of Physics (ed. M. Ghil, R. Benzi & G. Parisi), pp. 84–87. North Holland.

PLEWA, T., CALDER, A. C. & LAMB, D. Q. 2004 Type Ia supernova explosion: gravitationally confined detonation. *Astrophys. J.* **612**, L37.

PORTER, D., POUQUET, A. & WOODWARD, P. 2002 Measures of intermittency in driven supersonic flows. *Phys. Rev. E* **66**, 026301.

ROSNER, R., CALDER, A., DURSI, J., FRYXELL, B., LAMB, D. Q., NIEMEYER, J. C., OLSON, K., RICKER, P., TIMMES, F. X., TRURAN, J. W., TUFO, H., YOUNG, Y. N., ZINGALE, M., LUSK, E. & STEVENS, R. 2000 Flash code: Studying astrophysical thermonuclear flashes. *Comput. Sci. Engng* **2**, 33.

SAWFORD, B. L. 2001 Turbulent relative dispersion. *Annu. Rev. Fluid Mech.* **33**, 289.

SCHUMACHER, J. 2007 Sub-Kolmogorov-scale fluctuations in fluid turbulence. *Europhys. Lett.* **80**, 54001.

SCHUMACHER, J., SREENIVASAN, K. R. & YAKHOT, V. 2007 Asymptotic exponents from low-Reynolds-number flows. *New J. Phys.* **9**, 89.

SHE, Z.-S. & LÉVÊQUE, E. 1994 Universal scaling laws in fully developed turbulence. *Phys. Rev. Lett.* **72**, 336.

SHEN, X. & WARHAFT, Z. 2002 Longitudinal and transverse structure functions in sheared and unsheared wind-tunnel turbulence. *Phys. Fluids* **14**, 370.

SIROVICH, L., SMITH, L. & YAKHOT, V. 1994 Energy spectrum of homogeneous and isotropic turbulence in far dissipation range. *Phys. Rev. Lett.* **72**, 344.

TOSCHI, F. & BODENSCHATZ, E. 2009 Lagrangian properties of particles in turbulence. *Annu. Rev. Fluid Mech.* **41**, 375.

XU, H., BOURGOIN, M., OUELLETTE, N. T. & BODENSCHATZ, E. 2006 High-order Lagrangian velocity statistics in turbulence. *Phys. Rev. Lett.* **96**, 024503.

YAKHOT, V. & SREENIVASAN, K. R. 2004 Towards a dynamical theory of multifractals in turbulence. *Physica* A **343**, 147.

YAKHOT, V. & SREENIVASAN, K. R. 2005 Anomalous scaling of structure functions and dynamic constraints on turbulence simulations. *J. Stat. Phys.* **121**, 823.

YAMAZAKI, Y., ISHIHARA, T. & KANEDA, Y. 2002 Effects of wavenumber truncation on high-resolution direct numerical simulation of turbulence. *J. Phys. Soc. Japan* **71**, 777.

YEUNG, P. K. & POPE, S. B. 1989 Lagrangian statistics from direct numerical simulations of isotropic turbulence. *J. Fluid Mech.* **207**, 531.

YEUNG, P. K., POPE, S. B. & SAWFORD, B. L. 2006 Reynolds number dependence of Lagrangian statistics in large numerical simulations of isotropic turbulence. *J. Turbul.* **7**, N58.

WATANABE, T. & GOTOH, T. 2007 Inertial-range intermittency and accuracy of direct numerical simulation for turbulence and passive scalar turbulence. *J. Fluid Mech.* **590**, 117.

VAN DE WATER, W. & HERWEIJER, J. A. 1999 High-order structure functions of turbulence. *J. Fluid Mech.* **387**, 3.

WEIRS, G., DWARKADAS, V., PLEWA, T., TOMKINS, C. & MARR-LYON, M. 2005 Validating the flash code: vortex-dominated flows. *Astrophys. Space Sci.* **298**, 341.

ZHANG, J., MESSER, O. E. B., KHOKHLOV, A. M. & PLEWA, T. 2007 On the evolution of thermonuclear flames on large scales. *Astrophys. J.* **656**, 347.

ZHOU, T. & ANTONIA, R. A. 2000 Reynolds number dependence of the small-scale structure of grid turbulence. *J. Fluid Mech.* **406**, 81.

ZYBIN, K., SIROTA, V. A., ILYIN, A. S. & GUREVICH, A. V. 2008 Lagrangian statistical theory of fully developed hydrodynamical turbulence. *Phys. Rev. Lett.* **100**, 174504.